International Journal of Nanomedicine

Dovepress
open access to scientific and medical research

Open Access Full Text Article

ORIGINAL RESEARCH

Reduction-sensitive CD44 receptor-targeted hyaluronic acid derivative micelles for doxorubicin delivery

This article was published in the following Dove Press journal:
International Journal of Nanomedicine

Yishun Yang[1]
Yuan Zhao[2]
Jinshuai Lan[1]
Yanan Kang[3]
Tong Zhang[1]
Yue Ding[1]
Xinyu Zhang[1]
Lu Lu[3]

[1]Experiment Centre of Teaching and Learning, Shanghai University of Traditional Chinese Medicine, Shanghai, China; [2]Experiment Centre for Science and Technology, Shanghai University of Traditional Chinese Medicine, Shanghai, China; [3]School of Chinese Materia Medica, Shanghai University of Traditional Chinese Medicine, Shanghai, China

Introduction: A reduction-sensitive CD44-positive tumor-targetable drug delivery system for doxorubicin (DOX) delivery was developed based on hyaluronic acid (HA)-grafted polymers.

Materials and methods: HA was conjugated with folic acid (FA) via a reduction-sensitive disulfide linkage to form an amphiphilic polymer (HA-ss-FA). The chemical structure of HA-ss-FA was analyzed by ultraviolet spectroscopy, Fourier transform infrared spectroscopy, and ^{1}H nuclear magnetic resonance (NMR) spectroscopy. The molecular weight of HA-ss-FA was determined by high-performance gel permeation chromatography. Blank HA-ss-FA micelles and DOX-loaded micelles were prepared and characterized. The reduction responsibility, cellular uptake, and in vivo biodistribution of HA-ss-FA micelles were investigated.

Results: DOX-loaded micelles were of high encapsulation efficiency (88.09%), high drug-loading content (22.70%), appropriate mean diameter (100–120 nm), narrow size distribution, and negative zeta potential (−6.7 to −31.5 mV). The DOX release from the micelles was significantly enhanced in reduction environment compared to normal environment. The result of in vitro cytotoxicity assay indicated that the blank micelles were of low toxicity and good biocompatibility and the cell viabilities were >100% with the concentration of HA-ss-FA from 18.75 to 600.00 μg/mL. Cellular uptake and in vivo biodistribution studies showed that DOX-loaded micelles were tumor-targetable and could significantly enhance cellular uptake by CD44 receptor-mediated endocytosis, and the cellular uptake of DOX in CD44-positve A549 cells was 1.6-fold more than that in CD44-negative L02 cells. In vivo biodistribution of HA-ss-FA micelles showed that micelles were of good in vivo tumor targetability and the fluorescence of indocyanine green (ICG)-loaded micelles was 4- to 6.6-fold stronger than free ICG within 6 h in HCCLM3 tumor-bearing nude mice.

Conclusion: HA-ss-FA is a promising nanocarrier with excellent biocompatibility, tumor targetability, and controlled drug release capability for delivery of chemotherapy drugs in cancer therapy.

Keywords: hyaluronic acid, CD44 receptor targeting, redox responsive, folic acid, micelles, doxorubicin

Correspondence: Tong Zhang; Yue Ding
Experiment Centre of Teaching and Learning, Shanghai University of Traditional Chinese Medicine, 1200 Cailun Road, Pudong New District, Shanghai 201203, China
Tel +86 21 5132 2318; +86 21 5132 2325
Email zhangtdmj@hotmail.com; dingyue-2001@hotmail.com

Introduction

In recent years, nanoparticles have been attracting increasing attention in cancer therapy and cancer diagnosis.[1] For cancer treatment, the nanoparticles are widely used as carriers for delivery of antitumor drugs and show advantages in improving the solubility of cancer agents,[2] enhancing permeability and retention (EPR) effect,[3] increasing blood circulation,[4] and providing targeting strategies.[5]

submit your manuscript | www.dovepress.com
Dovepress
http://dx.doi.org/10.2147/IJN.S165359

Doxorubicin (DOX) is an effective broad spectrum chemotherapeutic agent in treating a variety of cancers, such as breast cancer, lung cancer, ovarian cancer, and liver cancer. However, it is known that DOX and other similar anthracycline derivatives have cardiotoxicity, which can be fatal in extreme cases.[6,7] And, there are other side effects of DOX, such as DNA damage and reactive oxygen species overproduction.[8] Therefore, the clinical application and therapeutic index of DOX and other anthracycline derivatives are largely limited by their severe adverse effects.[9,10] A method to minimize the side effects is by drug targeting. By loading DOX in a delivery system that selectively binds with cellular receptors overexpressed by the cancerous cells,[11] the delivery of DOX to the tumor region can be enhanced, the accumulation of DOX in the heart can be reduced, and the specificity of DOX can be improved.

Among all these nanocarriers, the amphiphilic polymers including a hydrophobic core and a hydrophilic shell are excellent candidates for carrying hydrophobic drugs.[12] Some of the amphiphilic polymers formed micelles in aqueous solution. The micelles encapsulate hydrophobic drugs and increase their solubility in water. Furthermore, special functions can be attached to these polymers, including linking the targeting group for target delivery and using environmentally responsive cross-linking agents for site-specific delivery.[1,13–15] Hyaluronic acid (HA) is a naturally occurring linear glycosaminoglycan that has many desirable properties for nanomedicine, such as biodegradability, biocompatibility, nontoxicity, and nonimmunogenicity.[11] It contains several chemical groups such as hydroxy and carboxy to which other components can be conjugated. In particular, the interaction between HA and CD44 receptor, which is overexpressed in many types of tumor cells' surface, makes it a promising molecule for application in a receptor-mediated targeting strategy.[16] Many studies have reported the application of HA as an active tumor-targeting ligand,[17–20] and it has been applied as a hydrophilic shell to nanodrug delivery systems, such as micelles.[21]

Folic acid (FA) is a prominent targeting molecule capable of specific interaction with FA receptor, which is also overexpressed in many kinds of tumor cells.[13,22–24] Despite there being many studies about nanoparticles that use HA and FA as targeting ligands to gain dual-CD44 and FA receptor-targeting ability in tumor delivery systems, other hydrophobic cores such as octadecyl were used in these reports.[25–28] Most of the hydrophobic cores in these reports were long-chain polymers. FA is widely used as a target ligand in nanoparticles including micelles, liposome, and others.[29] Generally, the hydrophobic core of these nanoparticles was long-chain polymer, so FA was in the part of the micelles' or liposome's shell for targeting purposes such as linking to the hydrophilic chain of these polymers. The inevitable use of long-chain polymers in the dual-targeting micelles and FA receptor-targeting micelles may cause problems in clinical application due to the poor biocompatibility and bioabsorbability of these polymers. As a kind of B vitamin, FA is absorbable and nontoxic to the human body. However, as FA has low solubility in water (0.01 mg/mL at 25°C), it can be used as a hydrophobic core of amphiphilic polymers, avoiding the use of other hydrophobic substances. It was reported that polymers synthesized by conjugating HA with small molecules such as deoxycholic acid (a hydrophobic substance) can form stable micelles.[30,31]

In this study, a CD44 receptor-targeted strategy was developed based on the self-assembly HA derivative to deliver DOX in cancer therapy (Figure 1). To synthesize HA-ss-FA conjugate, cystamine (CYS) which contains a reduction-sensitive disulfide bond was used as a cross-linking agent to link HA and FA. Reduction-sensitive micelles loading DOX were prepared and characterized. The encapsulation efficiency (EE) and the loading ability of DOX-loaded micelles were evaluated. The DOX release of DOX-loaded micelles in reduction environment was investigated. CD44 receptor-overexpressed human hepatocellular carcinoma HCCLM3 cells[32] and human lung adenocarcinoma A549 cells[4,16,33] were used to investigate the antitumor cytotoxicity in vitro and cellular uptake of the micelles. The antitumor effects of DOX-loaded micelles were evaluated by CellTiter 96® AQueous One Solution Cell Proliferation Assay ((3-(4,5-dimethylthiazol-2-yl)-5-(3-carboxymethoxyphenyl)-2-(4-sulfophenyl)- 2H-tetrazolium) [MTS] assay). The cellular uptake of DOX was determined using the confocal laser scanning microscopy (CLSM). Furthermore, the biodistribution of the micelles was studied in HCCLM3 tumor-bearing nude mice. The results showed that HA-ss-FA was a promising nanocarrier for the delivery of anticancer drugs to CD44 receptor-overexpressed tumors.

Materials and methods

Materials

Sodium hyaluronate (molecular weight [Mw] 21 kDa) was purchased from Bloomage Freda Biopharm Co., Ltd. (Jinan, China). The 1-Ethyl-3-(3-dimethylaminopropyl) carbodiimide hydrochloride (EDC), *N*-hydroxysuccinimide (NHS), and 2-(*N*-morpholino) ethanesulfonic acid (MES) were purchased from Yuanye Biological Technology Co., Ltd. (Shanghai, China). Dicyclohexylcarbodiimide (DCC), CYS dihydrochloride, reduced glutathione (GSH), and 2,4,6-trinitrobenzene

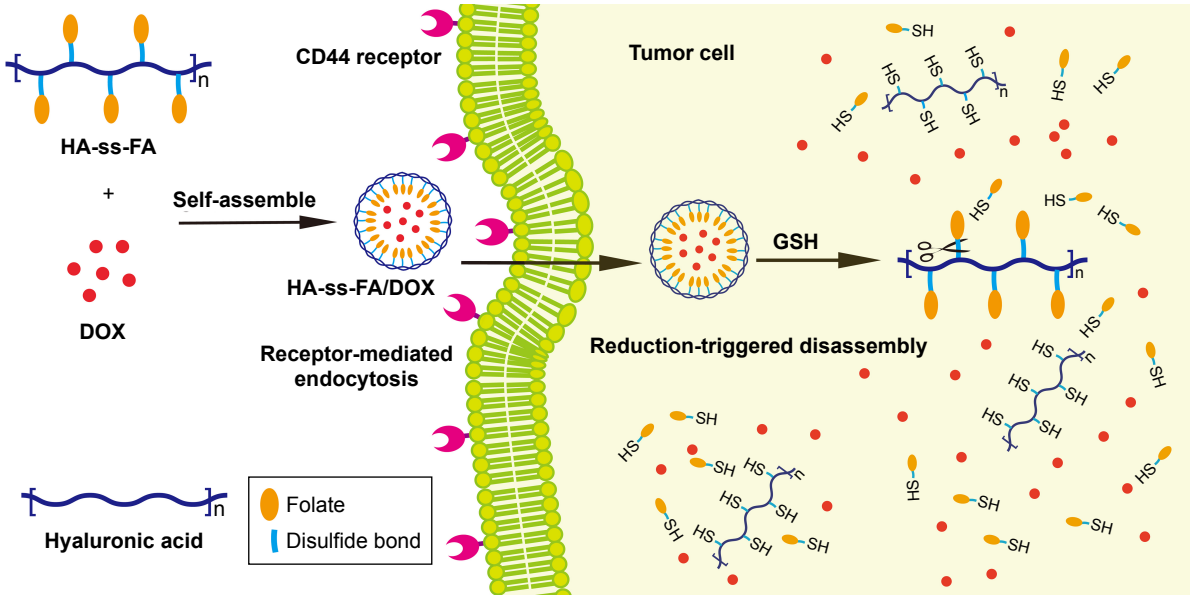

Figure 1 Illustration of HA-ss-FA/DOX micelles self-assembled from HA-ss-FA conjugate for CD44-targeted delivery of DOX into tumor cells.
Abbreviations: FA, folic acid; GSH, glutathione; HA, hyaluronic acid; DOX, doxorubicin.

sulfonic acid (TNBS) were purchased from Aladdin Biochemical Technology Co., Ltd. (Shanghai, China). DOX hydrochloride (DOX·HCl) was purchased from Meilun Biotech Co., Ltd. (Dalian, China). *N,N*-dimethylformamide (DMF) and dimethyl sulphoxide (DMSO) were purchased from Energy Chemical Co., Ltd. (Shanghai, China). The 4′,6-Diamidino-2-phenylindole (DAPI) was purchased from Beyotime Institute of Biotechnology (Shanghai, China). Indocyanine green (ICG) was purchased from Sigma-Aldrich Co. (St Louis, MO, USA). CellTiter 96® AQ_{ueous} One Solution Reagent (MTS) was purchased from Promega Corporation (Fitchburg, WI, USA). Dulbecco's Modified Eagle's Medium (DMEM) was purchased from Hyclone Laboratories, Inc. (Logan, UT, USA). Fetal bovine serum (FBS) was purchased from Biological Industries (Beit Haemek, Israel). CD44 mouse monoclonal antibody (mAb) was purchased from Cell Signaling Technology (Danvers, MA, USA). Fluorescein isothiocyanate (FITC) antimouse IgG antibody was purchased from BioLegend, Inc. (San Diego, CA, USA). Triethylamine (TEA), FA, and other reagents were purchased from Sinopharm Chemical Reagent Co., Ltd. (Beijing, China).

Synthesis of HA–CYS

A total of 400 mg of sodium hyaluronate was dissolved in 10 mL of MES buffer (0.1 M, pH 6.5). A total of 570 mg of EDC and 340 mg of NHS was added, and the reaction solution was stirred at 37°C for 15 min. Then, 340 mg of CYS was added and the reaction was allowed to proceed at 37°C for 2–12 h. The resulting solution was dialyzed (molecular weight cut off [MWCO] 3,500 Da) against NaCl solution (0.1 M) for 2 days and against distilled water for another 2 days, followed by lyophilization to obtain HA–CYS.[34,35] The structure of the product was verified by ^{1}H nuclear magnetic resonance (NMR) spectroscopy in D_2O (AVANCE 600 MHz; BrukerOptik GmbH, Ettlingen, Germany) and Fourier transform infrared (FITR) spectroscopy (Nicolet iS10; Thermo Fisher Scientific, Waltham, MA, USA).

Degree of amine substitution

To determine the degree of substitution (DS) of CYS in HA–CYS, free primary amino groups in CYS were quantified by the TNBS method.[36] The TNBS reagent reacts specifically with primary amino groups to form colored trinitrophenyl-amino acid derivatives.[37]

The TNBS reagent consisted of 0.1% (w/v) TNBS in water. L-Glycine (in the concentration range from 0.1 to 5.0 mM) was used to construct a standard curve. A total of 200 µL of sample solutions or standard solutions were added to the tubes. A total of 2 mL of sodium carbonate solution (4%) and 1 mL of TNBS reagent were then added to each tube, followed by mixing and incubating at 50°C for 1 h in the dark. After incubation, the reaction was cooled at room temperature and stopped by the addition of 0.5 N HCl (2 mL) to each tube. Samples were then sonicated for 10 min. Absorbance at 410 nm was measured using a UV–visible spectrophotometer (UV, 8454; Agilent Technologies, Santa Clara, CA, USA).

The concentration of HA was determined by the cetyltrimethyl ammonium bromide method as described by Chen and Wang.[38]

$$\text{DS of CYS (\%)} = \frac{\text{Concentration of free primary amino groups (mM)}}{\text{Concentration of HA (mM)}} \times 100 \quad (1)$$

Synthesis and characterization of HA-ss-FA

HA-ss-FA was synthesized in two steps (Figure 2). First, 0.1 g of FA was dissolved in 4 mL of anhydrous DMSO and 30 mg of NHS, 52 mg of DCC, and 40 µL of TEA were added. The mixture was stirred in the dark overnight. The precipitate generated during the reaction was removed by filtration. Then, 0.8 mL of filtrate was added to 44 mg of HA–CYS (DS =6.53, 17.37, or 45.36) suspension in 7 mL of DMF. The reaction proceeded at room temperature for 24 h in the dark. The product was purified by dialysis against 5% $NaHCO_3$ for 2 days and against distilled water for another 2 days to remove the impurities, followed by lyophilization. DS of FA in HA-ss-FA was determined by UV at the absorbance wavelength of 285 nm.

The chemical structure of the product was analyzed by UV, FTIR, and ^{1}H NMR in D_2O. The Mw of HA-ss-FA (DS of FA =7.49%) was measured by high-performance gel permeation chromatography (GPC) using HA as the standard. The assay was carried out after injecting 20 µL of sample to an Agilent 1260 HPLC System (Agilent Technologies) with a refractive index detector and a Shodex OHpak SB-804 HQ column (10 µm, 8.0 mm ×300 mm; Shodex, Tokyo, Japan). The column temperature was 40°C, and the mobile phase was 0.05 M Na_2SO_4 at a flow rate of 0.3 mL/min.[39]

In addition, to verify the reduction sensitivity of HA-ss-FA, 15 mg of HA-ss-FA was incubated with 20 mM GSH solution for 20 h. The resulting solution was dialyzed (MWCO 3,500 Da) against distilled water for 2 days and then

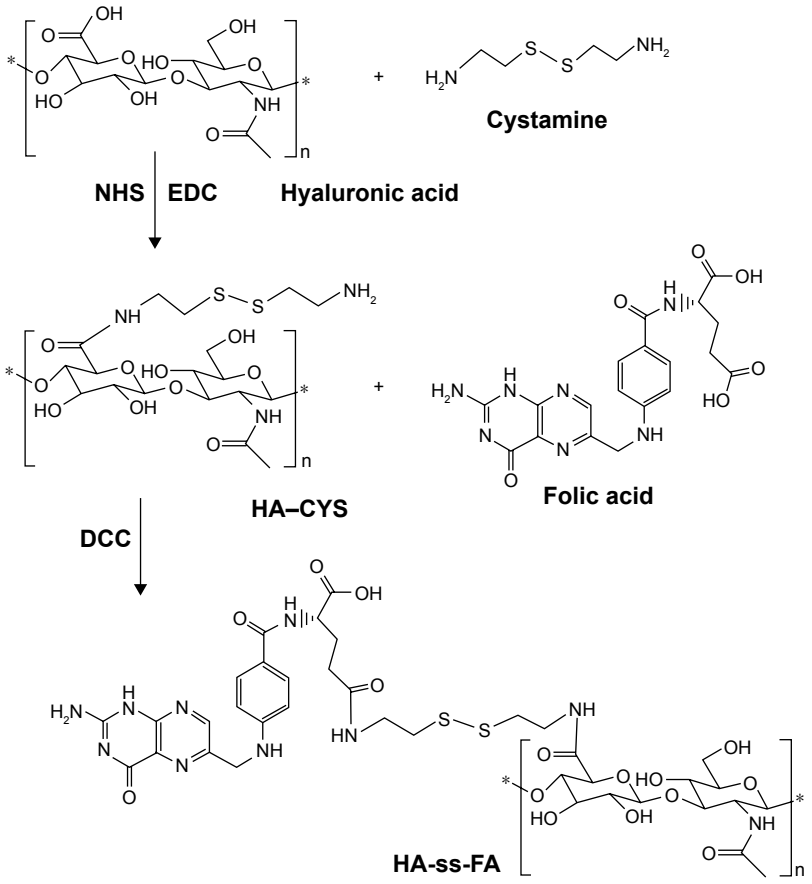

Figure 2 Synthesis pathway of HA-ss-FA conjugate.
Abbreviations: CYS, cystamine; DCC, dicyclohexylcarbodiimide; EDC, 1-ethyl-3-(3-dimethylaminopropyl) carbodiimide hydrochloride; FA, folic acid; HA, hyaluronic acid; NHS, *N*-hydroxysuccinimide.

filtered to remove the precipitate and lyophilized. The product (HA-ss-FA/GSH) was analyzed by UV and FTIR.

Determination of critical micelle concentration (CMC)

CMC of HA-ss-FA micelles was determined using pyrene as a fluorescence probe. Pyrene in acetone was added to a tube and evaporated at 40°C. HA-ss-FA solutions with different concentrations, varying from 0.001 to 0.500 mg/mL, were added and equilibrated for 12 h in the dark. The final concentration of pyrene was 6×10^{-7} M. The pyrene fluorescence spectra were measured using a fluorescence spectrophotometer (Cary Eclipse; Agilent Technologies) with the excitation wavelength of 335 nm and emission wavelength from 350 to 550 nm.

Preparation and characterization of HA-ss-FA micelles

Blank micelles were prepared by dissolving HA-ss-FA conjugate (1–10 mg/mL) in distilled water and then sonicating using a probe sonicator at 100 W in an ice bath for 10 min. DOX-loaded micelles were prepared by a dialysis method.[30,40] DOX·HCl (10 mg/mL) was dissolved in DMSO with three equivalent molar ratio of TEA and stirred in the dark overnight to obtain hydrophobic DOX (free base form DOX). HA-ss-FA conjugate (1–6 mg/mL) or HA (6 mg/mL, as a negative control) was dissolved in distilled water, and the above DOX solution was added at the weight ratio of HA-ss-FA:DOX =3:1 or HA:DOX =3:1. The mixtures were sonicated using a probe sonicator at 100 W in an ice bath for 10 min and then stirred in the dark for 4 h. The solution was dialyzed against distilled water for 6 h to remove DMSO and unreacted TEA, followed by centrifugation for 10 min at 3,500 rpm to remove the sediment (hydrophobic DOX).

After diluting 20 times with double distilled water, the particle size, polydispersity index (PDI), and zeta potential of the micelles were determined using a particle size and zeta potential analyzer (Zetasizer Nano ZS90; Malvern Instruments, Malvern, UK). The morphology of blank and DOX-loaded micelles was observed using transmission electron microscopy (TEM; JEM 2100; JEOL, Tokyo, Japan). The samples were prepared by dripping the solutions onto mesh copper grids with carbon film, then staining with 1% phosphotungstic acid, and drying in vacuum for 30 min.

To measure EE and drug loading (DL) content, DOX-loaded micelles were diluted with DMSO and sonicated to destroy the micellar structures. The content of DOX was determined using the UV–Vis spectrophotometer with the wavelength of 480 nm.

$$\text{EE}\,(\%) = \frac{\text{Weight of loaded DOX}}{\text{Weight of provided DOX}} \times 100 \quad (2)$$

$$\text{DL}\,(\%) = \frac{\text{Weight of loaded DOX}}{\text{Weight of DOX-loaded micelles}} \times 100 \quad (3)$$

The kinetic stability of DOX-loaded micelles was investigated.[41] Briefly, the micelles (1 mg/mL) were incubated with PBS (pH 7.4) or PBS containing 10% FBS and placed in a shaking incubator at 37°C (50 rpm). The size of the micelles was monitored at 0, 2, 6, 12, 24, and 48 h by a particle size and zeta potential analyzer.

In vitro reduction-triggered release of DOX from micelles

The release of DOX from DOX-loaded micelles was studied by a dialysis method in PBS (10 mM, pH 7.4) with or without 20 mM GSH.[41–43] Briefly, 1 mL of DOX-loaded micelles (at a DOX concentration of 20 μg/mL) was transferred to a dialysis bag (MWCO 3,500 Da; Spectrum Laboratories Inc., Milpitas, CA, USA) and then dialyzed against 40 mL of release medium in a tube. The tubes were placed in a shaking incubator at 37°C (100 rpm). A total of 5 mL of media was taken out, and an equivalent volume of fresh media was added at predetermined time intervals. The amount of released DOX was determined using a fluorescence spectrophotometer with the excitation wavelength of 480 nm and the emission wavelength of 560 nm.

Cell culture

HCCLM3 human liver cancer cells were obtained from Cold Spring Biotech Corp. (Taipei, China) as a gift;[44] the cells used were approved by the Ethics Committee of Shanghai University of Traditional Chinese Medicine (approval protocol number: 201804002). A549 human lung carcinoma cells were purchased from Cell Bank of Type Culture Collection of Chinese Academy of Sciences (Shanghai, China). L02 human hepatic cells were purchased from China Center for Type Culture Collection (Wuhan, China). The cells were cultured in DMEM with high glucose, supplemented with 10% FBS, 100 U/mL of penicillin, and 100 mg/mL of streptomycin. The cells were maintained at 37°C in a humidified incubator with 5% CO_2. The culture medium was changed every 2 days.

Detection of CD44 receptor expression on HCCLM3 and A549 cells

HCCLM3 and A549 cells were harvested and washed twice with PBS. A total of 10^6 cells were added in each tube, resuspended in 100 µL of diluted CD44 mouse mAb (prepared in PBS with 0.5% bovine serum albumin at the recommended dilution), and incubated for 2 h at room temperature. Then, the cells were washed with PBS three times and resuspended in 100 µL of diluted FITC antimouse immunoglobulin G (IgG) antibody (prepared in PBS at recommended dilution). After incubation for 30 min in the dark, the cells were washed with PBS three times, resuspended in 0.5 mL of PBS, and analyzed on a flow cytometer (FACSCalibur; BD Biosciences, San Jose, CA, USA). The data were analyzed using the FlowJo software V10 (Tree Star, Ashland, OR, USA).

In vitro cytotoxicity tests

Cytotoxicity of blank micelles and DOX-loaded micelles in HCCLM3 and A549 cells was evaluated by MTS assay. The cells were plated in a 96-well plate (8,000 cells/well) and incubated at 37°C in an atmosphere containing 5% CO_2 overnight. Then, the cell culture media was replaced with fresh media containing blank micelles, DOX·HCl, or DOX-loaded micelles with different concentrations and incubated for 48 h. The media was replaced by the mixture of 100 µL of fresh media and 20 µL of MTS. After incubating for 1 h, the absorbance was determined at 490 nm by a microplate reader (Eon; BioTek Instruments, Inc., Winooski, VT, USA). All experiments were repeated in triplicate. The cell viability was estimated, and IC_{50} values were calculated using the GraphPad Prism software (GraphPad Software, Inc., La Jolla, CA, USA).

Cellular uptake

CLSM was used to study cellular uptake and intracellular release behaviors of DOX-loaded micelles in HCCLM3 cells (CD44 receptor expressing positive cell line), A549 cells (CD44 receptor expressing positive cell line), and L02 cells (CD44 receptor expressing negative cell line, as negative control cells). Briefly, the cells were seeded at a density of 2×10^4 per well in glass bottom cell culture dishes (NEST Biotechnology Co., Ltd., Wuxi, China) and incubated for 24 h at 37°C. Then, 100 µL of DOX·HCl or DOX-loaded micelles (at a final DOX concentration of 10 µM) was added and incubated for 4 or 24 h. As inhibition experiments (negative control), free HA (5 mg/mL) or 1 µL of CD44 antibody was added with DOX-loaded micelles (at a final DOX concentration of 10 µM) and incubated for 4 or 24 h. The cells were washed twice with ice-cold PBS (pH 7.4) and fixed with 4% paraformaldehyde for 30 min, followed by washing with PBS three times. The cell nuclei were stained with 100 µL of DAPI (1 µg/mL) for 5 min and washed with PBS four times. The fluorescence images were captured by a laser scanning confocal microscope (TCS SP2; Leica Microsystems, Wetzlar, Germany). The fluorescence intensity of DOX in cells was analyzed by the LAS AF software (Leica Microsystems).

In vivo biodistribution test

Male BALB/c nude mice (Slac Laboratory Animal Co., Ltd, Shanghai, China), weighing 18–20 g, were quarantined in specific pathogen free animal laboratory with controlled humidity and temperature. All experiments adhered to the Guide for the Care and Use of Laboratory Animals[45] and were approved by the Ethics Committee of Shanghai University of Traditional Chinese Medicine (approval protocol number: 201803001). To investigate the in vivo distribution of HA-ss-FA micelles, the near-infrared fluorescent dye was used to prepare ICG-loaded micelles. HCCLM3 cells (4×10^6 per mouse) were subcutaneously injected into the right back of the mice. When the tumor size reached 800–900 mm^3, the mice were intravenously injected with free ICG and HA-ss-FA/ICG (at a concentration of 50 µg/mL). The in vivo fluorescent images were captured at 1, 3, 6, and 24 h using an in vivo imaging system (IVIS Lumina Series III; PerkinElmer Inc., Waltham, MA, USA) with the excitation and emission wavelengths of 780 and 800 nm, respectively. The mice were sacrificed 24 h after injection. The tumors and organs including heart, liver, spleen, lung, and kidney were collected to capture fluorescent images.

Statistical analyses

The experimental data are presented as the mean ± standard deviation (SD). Differences between groups were analyzed by Student's *t*-test or ANOVA. Differences were considered statistically significant when the *P*-values were <0.05.

Results and discussion

Synthesis and characterization of HA-ss-FA conjugate

HA-ss-FA conjugate was synthesized via a reduction-sensitive disulfide bond. CYS which contains a disulphide bond was used as a cross-linker. First, HA–CYS was synthesized by conjugating amine groups of CYS with carboxyl groups of HA in the presence of coupling agents EDC and NHS. According to the response surface methodology developed by Santhanam et al,[35] HA–CYS with different DS of CYS

Table 1 Influence of DS of CYS and FA in HA-ss-FA on physicochemical properties of DOX-loaded micelles (mean ± SD, n=3)

Sample	DS of CYS (%)	DS of FA (%)	Mean diameter (nm)	PDI	Zeta potential (mV)	EE (%)	DL (%)
HA-ss-FA_1	6.53	3.15	422.9±11.6	0.370±0.031	−51.5±0.2	22.32±0.04	6.87±0.02
HA-ss-FA_2	17.37	7.49	122.2±1.4	0.268±0.033	−31.5±0.7	49.25±0.56	14.01±0.16
HA-ss-FA_3	45.36	17.43	259.6±3.90	0.224±0.029	−28.3±2.2	63.03±0.18	17.19±0.09

Notes: The concentration of HA-ss-FA micelles was 1 mg/mL. The DS of CYS in HA-ss-FA_1,HA-ss-FA_2, HA-ss-FA_3 were 6.53, 17.37, and 45.36%, and the DS of FA in them were 3.15, 7.49, 17.43%, respectively.
Abbreviations: CYS, cystamine; DL, drug loading; DOX, doxorubicin; DS, degree of substitution; EE, encapsulation efficiency; FA, folic acid; HA, hyaluronic acid; PDI, polydispersity index; SD, standard deviation.

was synthesized by adjusting the reaction time. The DS of CYS in HA–CYS was determined by detecting free primary amino groups in CYS (TNBS method).[36] The DS of CYS was 6.53, 17.37, and 45.36% when reacted for 2, 6, and 12 h, respectively. As expected, the DS of CYS increased with the reaction time at 2–12 h.

Secondly, FA was conjugated with HA–CYS via amide bond. The HA–CYS with different DSs of CYS was used to synthesize HA-ss-FA, and the results of FA's DS are shown in Table 1. As the other conditions did not change, the DS of FA (3.15%–17.43%) increased with the DS of CYS (6.53%–45.36%), which indicated that FA was conjugated with HA via the CYS.

The chemical structure of HA-ss-FA was characterized by UV, ^{1}H NMR, and FTIR. UV spectra of HA, FA, and HA-ss-FA are shown in Figure 3A. There was no absorption peak of HA and an absorption peak of FA at 288 nm from 250 to 900 nm. HA-ss-FA showed an absorption peak at 285 nm. Compared to FA, the absorption peak of HA-ss-FA was slightly violet shifted (3 nm) due to the conjugation of amino in the HA–CYS molecules with carboxide in the FA molecules. The result indicated that FA had been conjugated with HA–CYS. And the DS of FA was determined by UV at 285 nm. ^{1}H NMR spectrum (Figure 4) of HA-ss-FA showed clear signals attributable to CYS at 3.00–2.71 ppm, and the characteristic proton peaks of FA appeared at 6.81, 7.65, 7.92, and 8.75 ppm. The characteristic proton peaks of HA were at 4.27–3.34 ppm, which were identical with a previous report.[46] The detailed analysis of HA-ss-FA ^{1}H NMR spectrum is tabulated in Table S1. FTIR spectrum is shown in Figure 5. The characteristic peaks of HA–CYS can be ascribed to 3,270 cm^{-1} for O–H stretching vibrations, 2,886 cm^{-1} for C–H stretching vibrations, 1,031 cm^{-1} for C–O stretching vibrations, and 1,333 cm^{-1} for C–H deformation vibration. And, there were obvious characteristic peaks of FA at 832 cm^{-1} (Ar–H deformation vibration of the aromatic ring) and 1,603–1,507 cm^{-1} (C=C skeletal vibration of the aromatic ring). Compared to the FTIR spectrum of FA, C=C skeletal vibration of the aromatic ring of HA-ss-FA FTIR spectrum moved from 1,694–1,605 to 1,603–1,507 cm^{-1}. The detailed analysis of HA-ss-FA FTIR spectrum is tabulated in Table S2. The FTIR spectrum was in accordance with a previous report.[47] The result suggested the successful conjugation of FA with HA. By combining with the result of UV, FTIR, and ^{1}H NMR spectra, the synthesis of HA-ss-FA was confirmed.[47]

Furthermore, the molecular weight of HA-ss-FA was determined by GPC (Figure 3B), the calculated number average molecular weight (M_n) was 24,217 Da (M_w/M_n=1.61). The

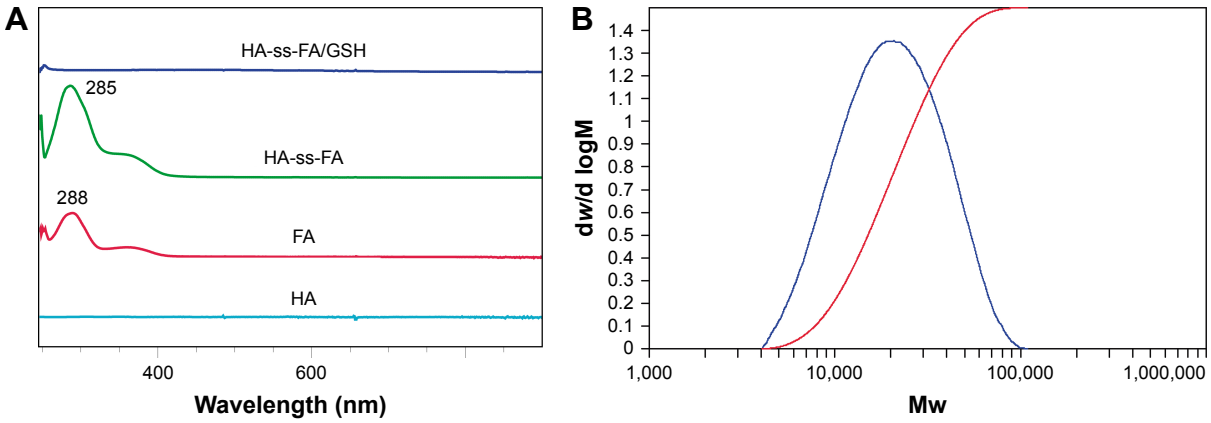

Figure 3 Characteristics of HA-ss-FA conjugate.
Notes: (**A**) UV–visible spectra of HA, FA, HA-ss-FA, and HA-ss-FA/GSH. (**B**) Differential relative molecular mass distribution plot of HA-ss-FA conjugate by high-performance gel permeation chromatography. HA-ss-FA/GSH, the lyophilized product of HA-ss-FA after treatment with GSH.
Abbreviations: CYS, cystamine; FA, folic acid; HA, hyaluronic acid; GSH, glutathione; Mw, molecular weight; UV, ultraviolet.

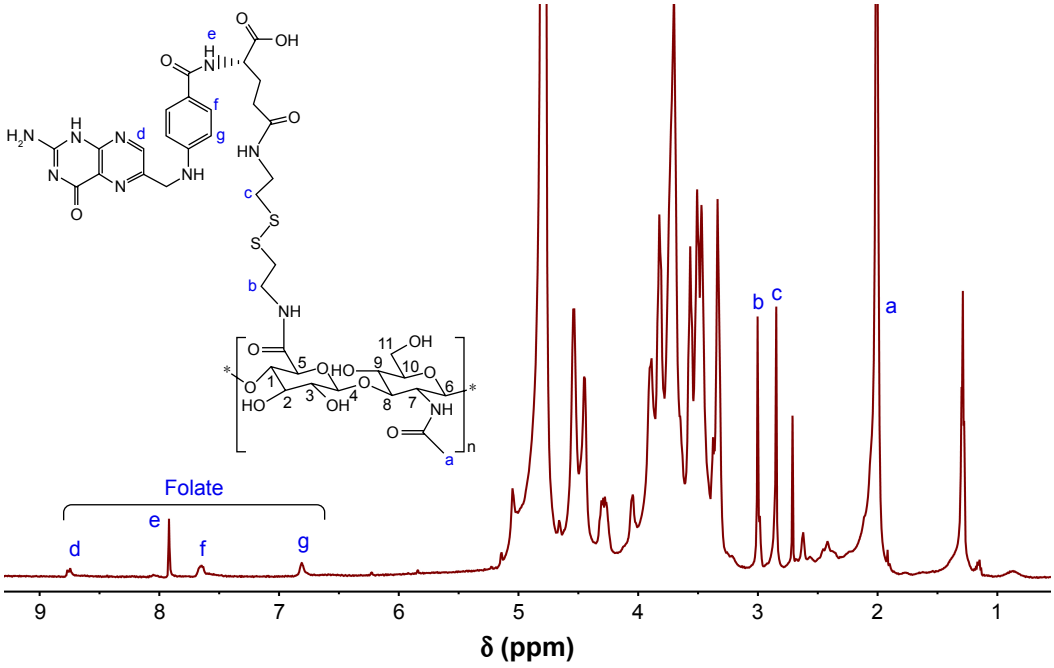

Figure 4 ^{1}H NMR spectrum of HA-ss-FA conjugates in deuterium oxide (600 MHz).
Note: a–g represent the characteristic proton peaks and the corresponding atomic numbers in HA-ss-FA.
Abbreviations: FA, folic acid; HA, hyaluronic acid; NMR, nuclear magnetic resonance.

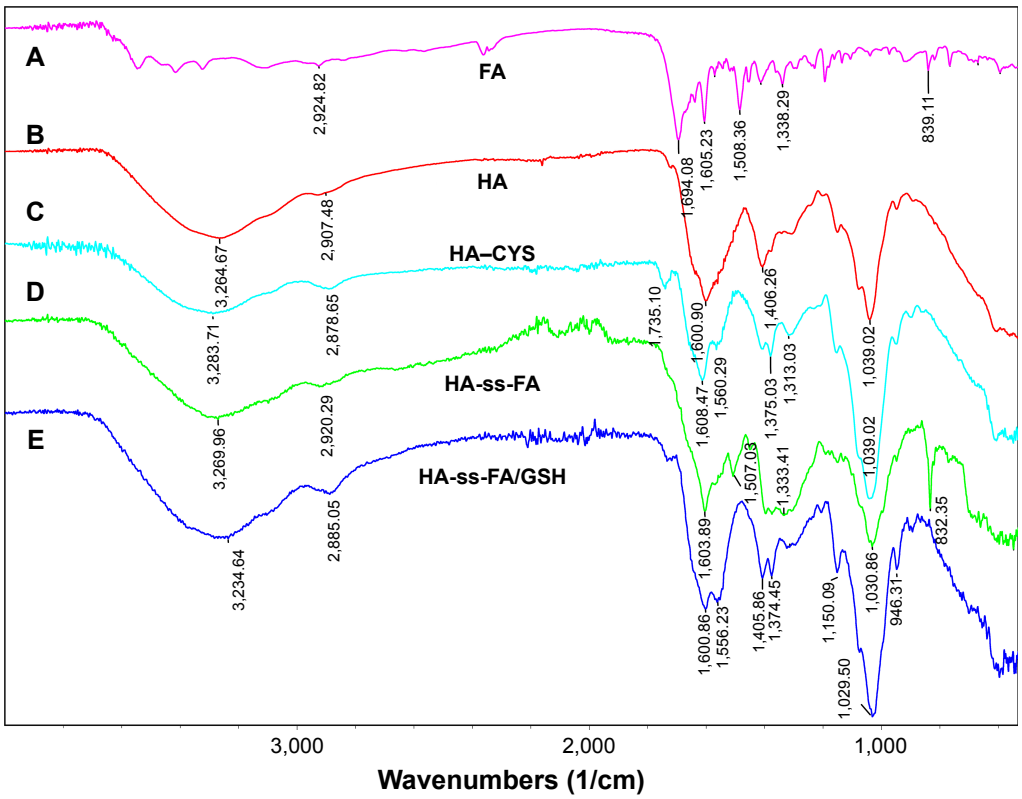

Figure 5 FTIR spectrum of (**A**) FA, (**B**) HA, (**C**) HA–CYS, (**D**) HA-ss-FA conjugate, and (**E**) the lyophilized product of HA-ss-FA after incubation with 20 mM GSH solution for 20 h.
Note: HA-ss-FA/GSH, the lyophilized product of HA-ss-FA after treatment with GSH.
Abbreviations: CYS, cystamine; FA, folic acid; FTIR, Fourier transform infrared; GSH, glutathione; HA, hyaluronic acid.

Mw of HA-ss-FA was close to the original HA (21 kDa). Compared with HA, increasing of the Mw of HA-ss-FA suggested that the conjugation of CYS (17.37%) and FA (7.49%) was successful.

In addition, the reduction sensitivity of HA-ss-FA was verified. As the disulfide linkage of HA-ss-FA was supposed to be broken by GSH, HA-ss-FA was incubated with 20 mM GSH and the product was analyzed by UV and FTIR. The spectra of the product (HA-ss-FA/GSH) are shown in Figure 3A. UV spectrum (Figure 3A) showed that after treating with GSH, the absorption peak of HA-ss-FA disappeared at 285 nm and the UV spectrum of HA-ss-FA/GSH was similar to the UV spectrum of HA. This result demonstrated that the HA-ss-FA was cleaved by GSH via the disulfide linkage and FA was removed as a precipitate. To further confirm the degradation of HA-ss-FA by GSH, the product (HA-ss-FA/GSH) was analyzed by FTIR. As shown in Figure 5, the FTIR spectrum of HA-ss-FA/GSH showed the clearly characteristic peaks of HA–CYS at 1,608, 1,560, 1,375, 1,039 cm^{-1} (Table S2). However, the benzene ring characteristic peaks of FA no longer existed at 1,507 and 832 cm^{-1}. The result verified that HA-ss-FA was degraded by GSH via the disulfide linkage, which indicated that HA-ss-FA was redox sensitive.

Preparation and characterization of HA-ss-FA micelles

DOX-loaded micelles with different DSs of FA in HA-ss-FA were prepared and characterized. As shown in Table 1, the size of these micelles ranged from 128.4 to 422.9 nm within the DS of FA from 3.15 to 11.19%. The physicochemical properties, EE, and DL of these micelles are listed in Table 1. The mean diameter of DOX-loaded micelles was apparently influenced by the DS of FA, and the valley value (122.2 nm) appeared when the DS of FA was 7.49%. The size and PDI of HA-ss-FA_1 (DS of FA =3.15%) were the largest, probably because the hydrophobic strength was weaker with less micellar core. As the hydrophobic strength became much stronger with more micellar core, the EE and DL increased with the DS of FA. Similar results were reported by Liu et al.[27] The PDI changed insignificantly (0.224–0.268) with the DS of FA from 7.49 to 17.43%; both HA-ss-FA_2 (DS of FA =7.49%) and HA-ss-FA_3 (DS of FA =17.43%) had narrow size distribution. Besides, the zeta potential was obviously affected by the DS of FA and the value increased from −51.5 to −28.3. The zeta potential of the micelles was negative because of the carboxylic acid moieties (COO^-) in HA, which are present on the surface of the micellar particles.[48] The reason for HA-ss FA becoming less negatively charged was because the more negatively charged carboxyl group of HA was replaced by CYS and FA. However, the particle size of HA-ss-FA_3 was much larger than HA-ss-FA_2, probably because the larger Mw of HA-ss-FA leads to larger size. It has been reported that nanoparticles are more likely to escape filtration by liver and spleen and enhance the EPR effect, but the probability of entrapment within liver and spleen increased when the size of nanoparticles was >150 nm.[49,50] Moreover, neutral and slightly negatively charged nanoparticles have longer circulation lifetimes and less clearance by the mononuclear phagocyte system (MPS) than positively charged nanoparticles.[51,52] For overall consideration, HA-ss-FA_2 seemed to be more suitable for tumor-targeting delivery owing to its appropriate particle size.

Blank micelles with different concentrations were prepared and characterized. The mean diameter (Figure 6A), PDI, and zeta potential of HA-ss-FA micelles were measured and are listed in Table 2. The mean diameter of blank micelles was from 125.4 to 231.7 nm, which varied with the concentration of HA-ss-FA conjugate. Although the size of the micelles was the smallest (125.4 nm) at 1 mg/mL, the PDI was the largest, which indicated that the size distribution was wide at 1 mg/mL. The size of the micelles was 231.7 nm at 10 mg/mL, which was too large and not suitable for tumor-targeting delivery. The size, PDI, and zeta potential of the micelles were 127.4 nm, 0.237, and −30.0 mV at 6 mg/mL, and were of narrow size distribution and appropriate size for tumor-targeting delivery. The negative zeta potential of the micelles (−30.0 mV at 6 mg/mL) could provide a repelling force between particles and increase the stability of the micelles.[53,54]

DOX-loaded micelles with different concentrations were prepared and characterized. As shown in Table 3, the particle size of DOX-loaded micelles was 112.7–103.7 nm (Figure 6C), which was smaller than blank micelles. This was probably because the encapsulated hydrophobic drug increased the hydrophobic interaction between DOX and FA groups in HA-ss-FA; thus, the micelle core became more hydrophobic and the micelles shrunk.[55,56] The particle size of DOX-loaded micelles changed slightly with the concentration of HA-ss-FA conjugate, and the zeta potential was negative from −6.7 to −31.5 mV. The EE and DL ranged from 46.30 to 88.09 and 13.25 to 22.70% when the concentration of HA-ss-FA increased from 1 to 6 mg/mL. When the HA-ss-FA concentration was 6 mg/mL, DOX was encapsulated into the hydrophobic core of the micelles with high efficiency (the EE and DL were 88.09 and 22.70%, respectively). Because HA is negatively charged[54] and may associate with the positively

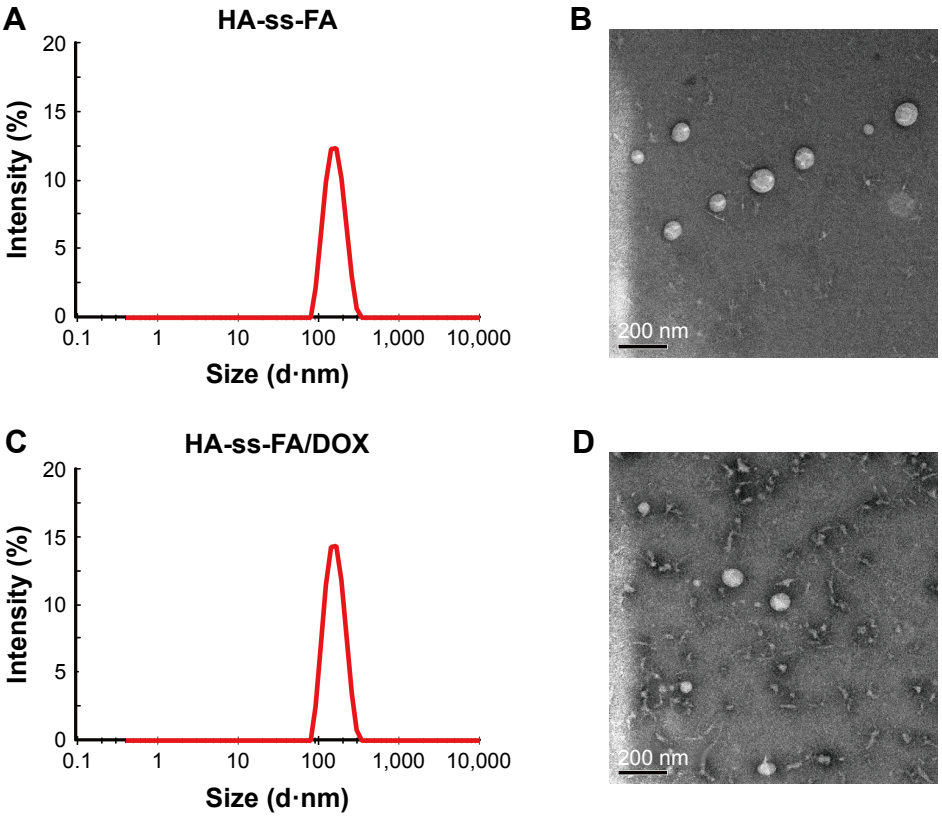

Figure 6 Size distribution and TEM micrograph of HA-ss-FA micelles.
Notes: Size distribution of (**A**) HA-ss-FA micelles and (**C**) HA-ss-FA/DOX micelles by DLS. The concentration of HA-ss-FA conjugate was 6 mg/mL. TEM micrograph of (**B**) HA-ss-FA micelles and (**D**) HA-ss-FA/DOX micelles.
Abbreviations: DLS, dynamic light scattering; DOX, doxorubicin; FA, folic acid; HA, hyaluronic acid; TEM, transmission electron microscopy.

charged DOX, a control experiment that used HA (6 mg/mL) associated with DOX (HA/DOX) following the same steps as the preparation of DOX-loaded micelles, was performed. The DL of DOX in HA/DOX was only 0.68%, which was far less than for HA-ss-FA/DOX. The result indicated that the electrostatic interactions between HA and DOX were not strong enough to bind DOX to HA or HA-ss-FA. Therefore, DOX was encapsulated in the micelles rather than associated with HA by electrostatic interactions.

HA-ss-FA conjugate was self-assembled, and micelles were formed in aqueous conditions. The CMC of the HA-ss-FA was 0.036 mg/mL by fluorescence spectra using pyrene as a fluorescence probe (Figure 7A). The low CMC value indicates that the micelles form at a low concentration, which ensured that the micelles can retain their original morphology under highly diluted conditions.[20,57] Furthermore, the kinetic stability of DOX-loaded micelles was investigated.[41] The result (Figure 7B) showed that the size changes in the micelles in PBS (range from 130 to 192 nm) and PBS containing 10% FBS (range from 124 to 177 nm) were not significant within 48 h. The result suggested that the micelles were stable in physiological environment.[41] Moreover, there was no significant difference between PBS and PBS containing 10% FBS, which indicated that the micelles were stable in the presence of FBS.

Table 2 Influence of HA-ss-FA concentration on the physicochemical properties of blank micelles (mean ± SD, n=3)

Concentration of HA-ss-FA (mg/mL)	Mean diameter (nm)	PDI	Zeta potential (mV)
1	125.4±1.6	0.392±0.020	−11.2±1.5
6	127.4±7.3	0.237±0.050	−30.0±6.3
10	231.7±1.5	0.278±0.100	−44.5±2.6

Note: The DS of HA-ss-FA was 7.49%.
Abbreviations: DS, degree of substitution; FA, folic acid; HA, hyaluronic acid; PDI, polydispersity index; SD, standard deviation.

The particle morphology of blank and DOX-loaded micelles was observed by TEM (Figure 6B and D). The TEM micrograph demonstrated that the micelles were near spherical in shape. The size was smaller than that determined by DLS. The reason was probably due to the different states of micelles in these two determinations. The TEM samples were dried, and the micelles may shrink during drying.[58]

Table 3 Influence of HA-ss-FA concentration on the physicochemical properties of DOX-loaded micelles (mean ± SD, n=3)

Concentration of HA-ss-FA (mg/mL)	Mean diameter (nm)	PDI	Zeta potential (mV)	EE (%)	DL (%)
1	112.7±1.0	0.128±0.030	−31.5±1.2	46.30±1.61	13.25±0.40
3	118.8±3.8	0.161±0.010	−6.7±1.5	82.94±2.77	21.66±0.57
6	103.7±5.0	0.187±0.050	−18.9±1.3	88.09±2.54	22.70±0.51

Note: The DS of HA-ss-FA was 7.40%.
Abbreviations: DL, drug loading; DOX, doxorubicin; DS, degree of substitution; EE, encapsulation efficiency; FA, folic acid; HA, hyaluronic acid; PDI, polydispersity index; SD, standard deviation.

In vitro reduction-triggered drug release of DOX

The release of DOX from DOX-loaded micelles was investigated in PBS (pH 7.4) at 37°C with or without 20 mM GSH, simulating the biological environment inside the tumor cells.[59] The result is shown in Figure 7C; DOX release from the micelles in the presence of 20 mM GSH was faster than in the absence of GSH due to the fracture of the disulfide bond in HA-ss-FA molecules in the reductive environment, and the released amount of DOX in PBS with 20 mM GSH was 1.4-fold more than in PBS without GSH, at 27 h. The result suggested that the HA-ss-FA micelles were reduction sensitive and would release rapidly in tumor cells.

CD44 receptor expression on HCCLM3 and A549 cells

The CD44 receptor expression on HCCLM3 and A549 cells was determined by a flow cytometer. As shown in Figure 8, both HCCLM3 and A549 cells expressed CD44 receptor and the CD44 receptor expression proportion of HCCLM3 and A549 cells was 71.5 and 89.8%, respectively. The result indicated that HCCLM3 and A549 cells were appropriate cell lines to study CD44 receptor-targeting delivery effect of nanoparticles. And, the mean fluorescence intensity (MFI) of HCCLM3 and A549 cells was 917 and 362, respectively, which suggested that the expression level of CD44 receptors on the surface of A549 cells was much higher (~2.5-fold higher) than for HCCLM3 cells.

In vitro cytotoxicity tests

The in vitro cytotoxicity of blank micelles and DOX-loaded micelles on HCCLM3 and A549 cells was evaluated by MTS assay. As shown in Figure 9A and C, the result showed that blank micelles with the concentration of 18.75–600.00 μg/mL, which was much larger than the dose of drug-loaded micelles, were nontoxic (the cell viabilities were >100%) against HCCLM3 and A549 cells. This indicated that HA-ss-FA was of excellent biocompatibility and good biological safety. As shown in Figure 9B and D, the antitumor effect of DOX·HCl and DOX-loaded micelles was dependent on the drug concentration. However, the result showed that the DOX-loaded micelles had weaker cell inhibition efficacy compared to DOX·HCl. The half-maximal inhibitory concentration (IC_{50}) values of DOX·HCl

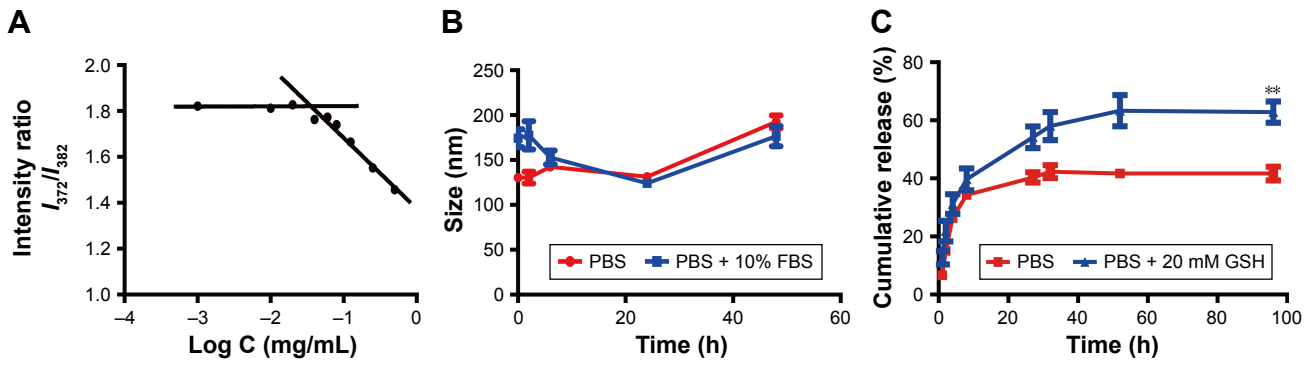

Figure 7 Characteristics of HA-ss-FA micelles.
Notes: (**A**) Determination of CMC of HA-ss-FA micelles using pyrene as a fluorescence probe. Intensity ratio ($I_{372\ nm}/I_{382\ nm}$) in the pyrene emission spectra is plotted versus concentration of HA-ss-FA conjugate. (**B**) Stability of HA-ss-FA/DOX micelles in PBS (pH 7.4) and PBS containing 10% FBS. (**C**) Reduction-triggered release of DOX from HA-ss-FA/DOX at 37°C in PBS (pH 7.4) and PBS containing 20 mM GSH for 96 h (mean ± SD, n=3). $^{**}P<0.01$.
Abbreviations: CMC, critical micelle concentration; DOX, doxorubicin; FA, folic acid; FBS, fetal bovine serum; GSH, glutathione; HA, hyaluronic acid; I, intensity; PBS, phosphate-buffered solution; SD, standard deviation.

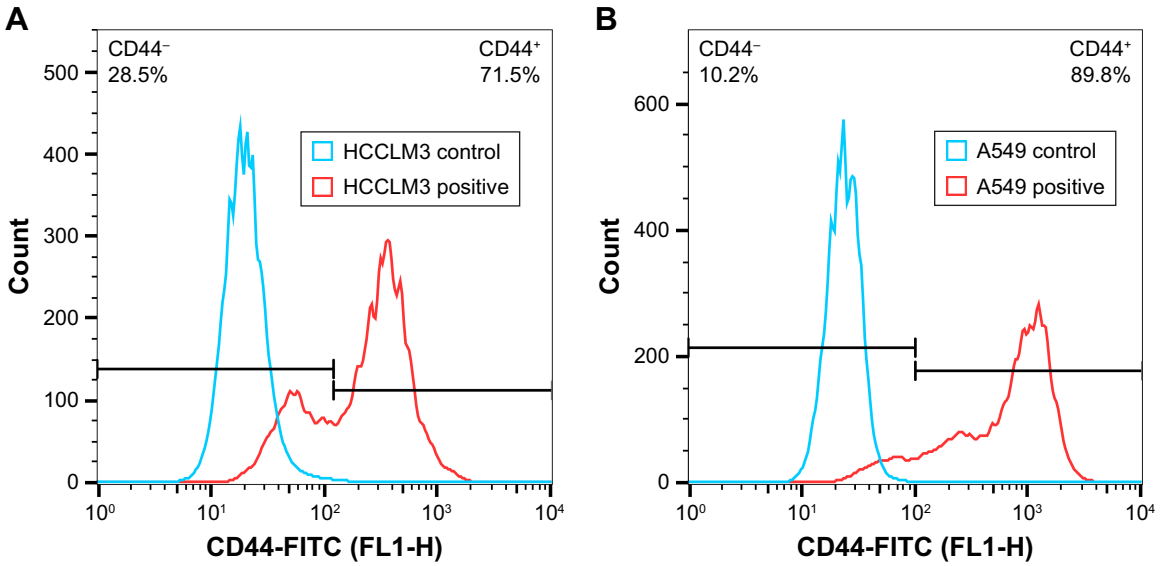

Figure 8 Detection of CD44 receptor expression on (**A**) HCCLM3 and (**B**) A549 cells.
Abbreviation: FITC, fluorescein isothiocyanate.

were 2.29 and 0.53 μM against HCCLM3 and A549 cells, while the IC_{50} values of HA-ss-FA/DOX micelles (DOX-loaded micelles) were 4.24 and 1.31 μM against HCCLM3 and A549 cells, respectively. This was probably because DOX·HCl was water soluble and could be transported into cells quickly by a passive-diffusion mechanism, whereas the drug-loaded micelles were internalized via endocytosis effect, which delayed the drug release of DOX in the micelles.

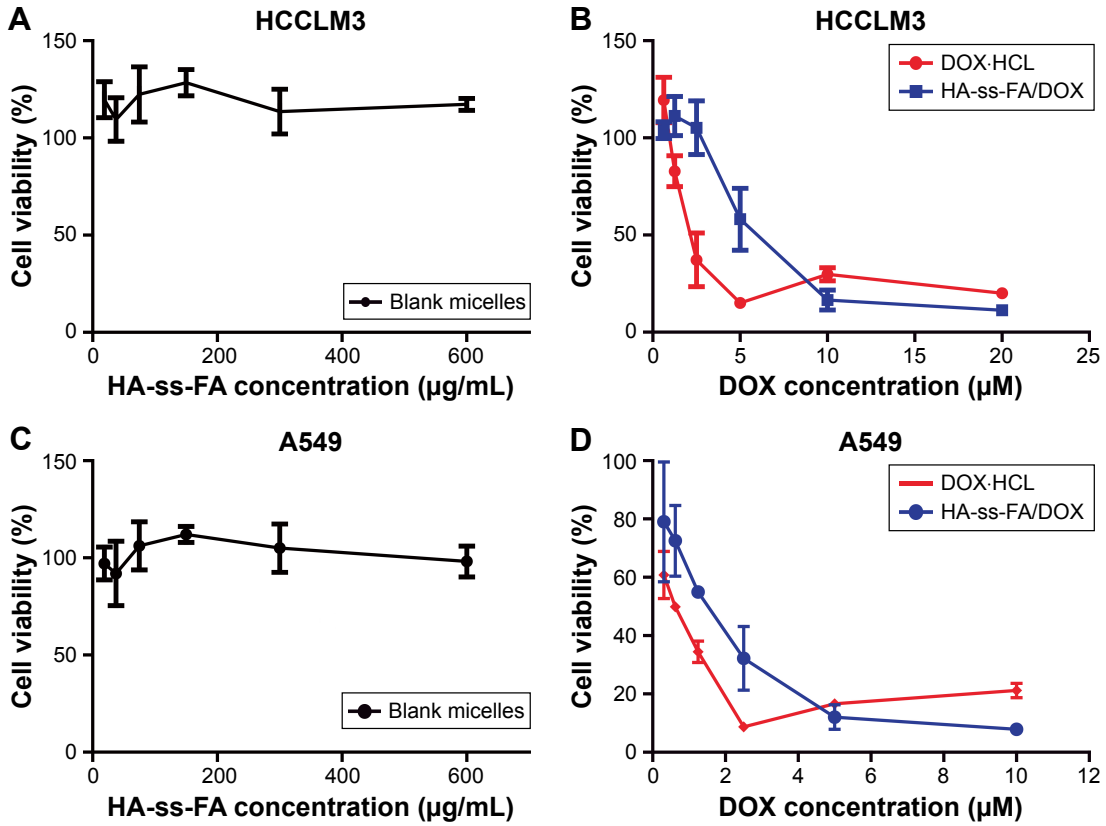

Figure 9 In vitro cytotoxicity of blank micelles and DOX-loaded micelles on HCCLM3 and A549 cells.
Notes: (**A**) HCCLM3 cells were incubated with HA-ss-FA micelles, (**B**) DOX·HCl and DOX-loaded micelles for 48 h (mean ± SD, n=3). (**C**) A549 cells were incubated with HA-ss-FA micelles, (**D**) DOX·HCl and DOX-loaded micelles for 48 h (mean ± SD, n=3).
Abbreviations: DOX, doxorubicin; DOX·HCl, DOX hydrochloride; FA, folic acid; HA, hyaluronic acid; SD, standard deviation.

Similar results were reported previously.[60,61] In contrast, when the concentration of DOX reached 5–10 μM, DOX-loaded micelles showed stronger inhibition efficacy than DOX·HCl, which was probably because the passive diffusion speed of DOX·HCl was restricted at a high concentration owing to saturation, whereas the endocytosis speed of the micelles was not affected by high concentration.

Cellular uptake of DOX-loaded micelles

The uptake and intracellular release of DOX·HCl and DOX-loaded micelles in HCCLM3 cells were studied using CLSM. The cells were incubated with DOX·HCl and HA-ss-FA/DOX for 4 or 24 h. In addition, the cells were incubated with an excess amount of HA and DOX-loaded micelles as a negative control (HA-ss-FA/DOX + HA group, an inhibition test) to confirm the CD44 receptor-mediated endocytosis of the micelles, according to a previous report.[58] HA-ss-FA/DOX + HA group showed the weakest DOX fluorescence among the three groups. This indicated that the micelles were endocytosed by HCCLM3 cells via CD44 receptor-mediated endocytosis. Interestingly, as shown in Figure 10A, there was no significant difference between cells incubated with DOX·HCl and DOX-loaded micelles for 4 h. However, after 24 h incubation, DOX fluorescence was stronger in the cells of the DOX-loaded micelles group than in the DOX·HCl group

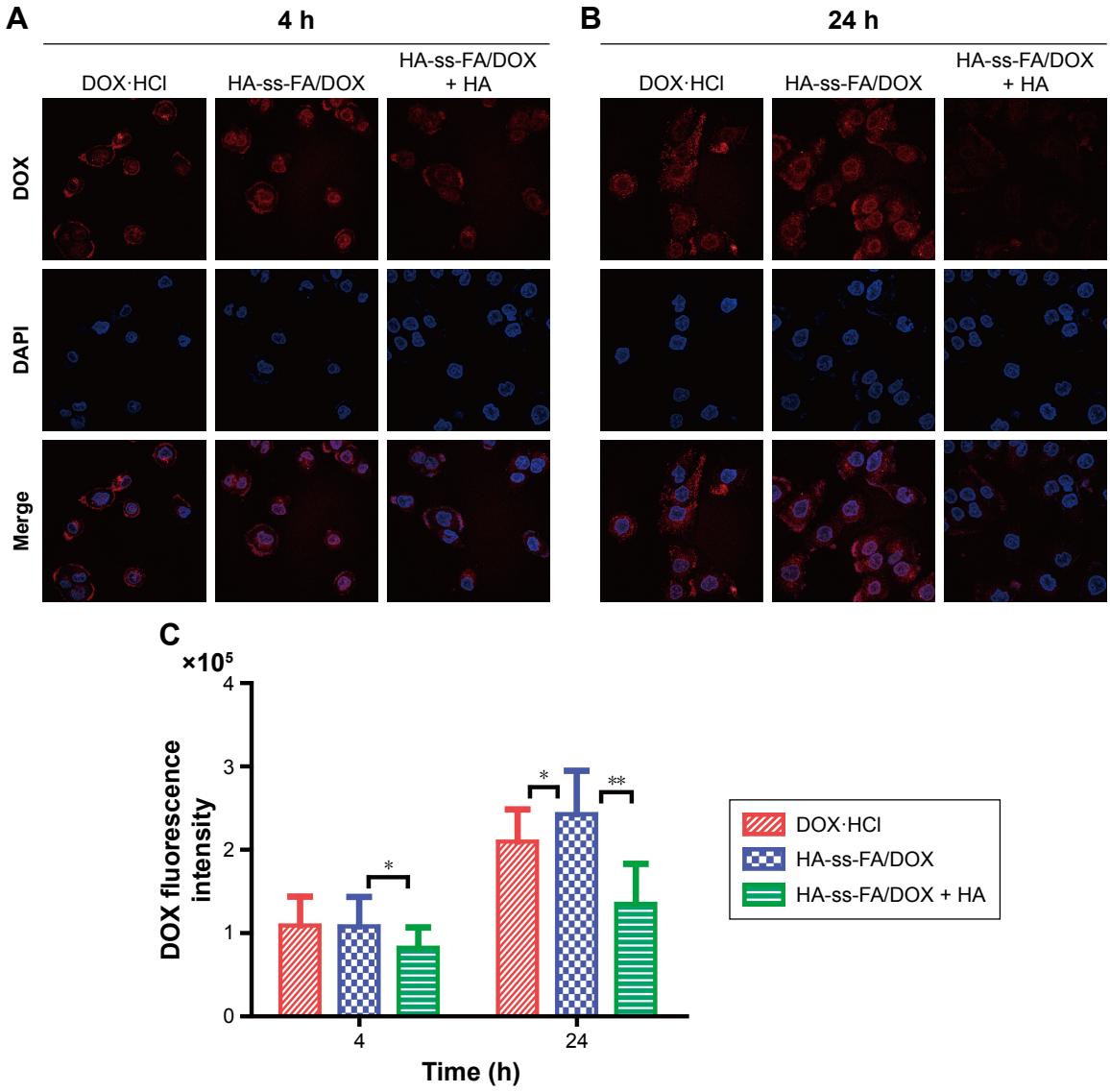

Figure 10 Cellular uptake study of DOX·HCl and HA-ss-FA/DOX micelles in HCCLM3 cells using CLSM.
Notes: CLSM images of HCCLM3 cells incubated with DOX·HCl, HA-ss-FA/DOX, and HA-ss-FA/DOX with free HA (5 mg/mL, inhibition experiment as a negative control) for (**A**) 4 and (**B**) 24 h. (**C**) Mean fluorescence intensity of DOX in HCCLM3 cells incubated with DOX·HCl, HA-ss-FA/DOX, and HA-ss-FA/DOX with free HA (5 mg/mL) for 4 and 24 h (mean ± SD, n=20). *$P<0.05$. **$P<0.01$.
Abbreviations: CLSM, confocal laser scanning microscopy; DAPI, 4′,6-diamidino-2-phenylindole; DOX, doxorubicin; DOX·HCl, DOX hydrochloride; FA, folic acid; HA, hyaluronic acid; SD, standard deviation.

(Figure 10B). This was probably because DOX·HCl diffused into the cells through passive diffusion without a release process and DOX-loaded micelles were internalized by the cells via a CD44 receptor-mediated endocytosis mechanism with a reduction-triggered release process,[62] which delayed the release of DOX in the first 4 h. The result demonstrated that the micelles effectively enhanced the cellular uptake of DOX-loaded micelles within 24 h. The fluorescent intensity of DOX in HCCLM3 cells was calculated by the LAS AF software. As shown in Figure 10C, compared with DOX·HCl, the uptake of HA-ss-FA/DOX increased 15.81% after 24 h incubation ($P<0.05$).

To confirm the CD44 receptor-mediated endocytosis of HA-ss-FA micelles, we investigated the cellular uptake of DOX-loaded micelles in A549 cells and L02 cells (negative control); the results are shown in Figure 11. Interestingly, after incubating with DOX·HCl or HA-ss-FA/DOX for 4 h, the DOX fluorescence of the HA-ss-FA/DOX group in A549 cells was the strongest, even stronger (1.3-fold stronger) than DOX·HCl group ($P<0.001$), which was different from the cellular uptake test result of HCCLM3 cells. As the CD44 expression level of A549 cells was much higher than HCCLM3 (~2.5-fold higher), it seems reasonable that the cellular uptake of A549 cells was higher than HCCLM3 cells. HA-ss-FA/DOX with CD44 antibody was incubated with A549 for 4 h and observed by CLSM as a negative control (inhibition experiment); the DOX fluorescence was significantly weaker (2.1-fold weaker) than HA-ss-FA/DOX without CD44 antibody ($P<0.001$), as expected. This result indicated that HA-ss-FA/DOX was internalized by the cells via a CD44 receptor-mediated endocytosis. Similar to the inhibition experiment of HA-ss-FA/DOX with HA in HCCLM3 cells, the DOX fluorescence of DOX·HCl was stronger than HA-ss-FA/DOX with CD44 antibody in A549 cells due to the delayed release of DOX from DOX-loaded micelles within 4 h. Furthermore, CD44 receptor expression negative L02 cells were incubated with HA-ss-FA/DOX for 4 h as a negative control and the DOX fluorescence of HA-ss-FA/DOX in L02 cells was obviously weaker (1.6-fold weaker) than that in A549 cells ($P<0.001$). These results demonstrated that the cellular uptake of HA-ss-FA/DOX was mediated by CD44 receptor in CD44 highly expressing cells owing to the CD44-targeting ability of HA.

In vivo biodistribution

To evaluate the biodistribution of HA-ss-FA micelles in vivo, ICG was loaded in HA-ss-FA micelles and injected intravenously to HCCLM3 tumor-bearing nude mice. The EE and DL were 70.01 and 10.46%, respectively. The fluorescence images (Figure 12A) showed obvious

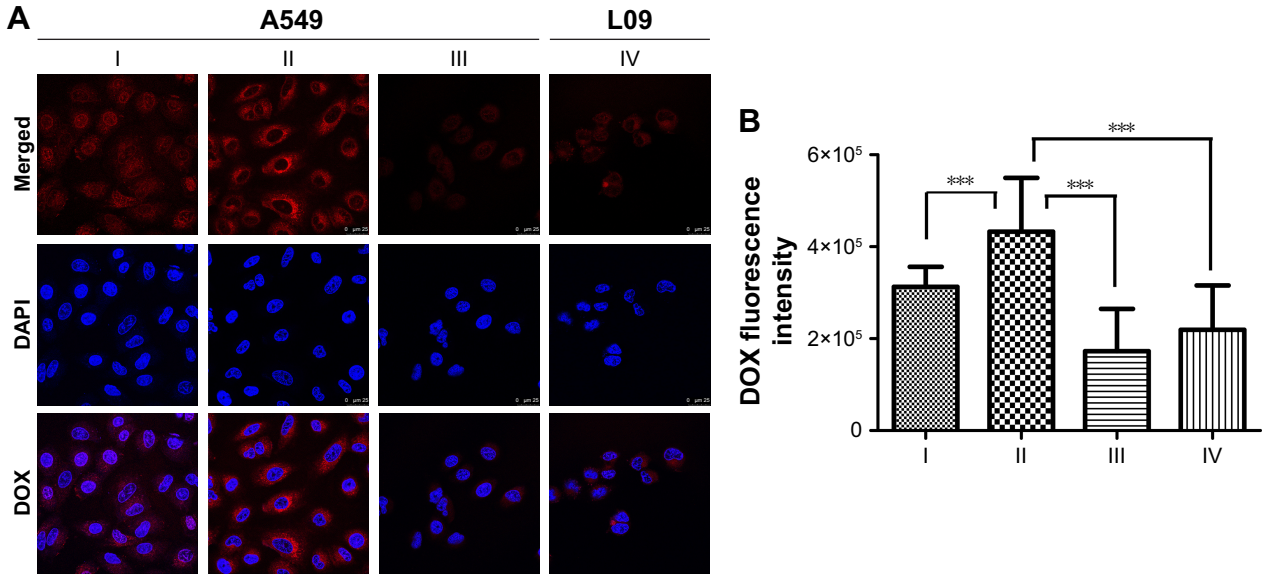

Figure 11 Cellular uptake study of DOX·HCl and HA-ss-FA/DOX micelles in A549 cells and L02 cells using CLSM.

Notes: (**A**) CLSM images of A549 cells incubated with (I) DOX·HCl, (II) HA-ss-FA/DOX, and (III) HA-ss-FA/DOX with CD44 antibody (inhibition experiment as a negative control) for 4 h and (IV) L02 cells (CD44 receptor expression negative cell line, as a negative control) incubated with HA-ss-FA/DOX for 4 h. Magnification ×400. (**B**) Mean fluorescence intensity of DOX in A549 cells incubated with (I) DOX·HCl, (II) HA-ss-FA/DOX, and (III) HA-ss-FA/DOX with free CD44 antibody for 4 h, and (IV) L02 cells incubated with HA-ss-FA/DOX for 4 h (mean ± SD, n=20). ***$P<0.001$.

Abbreviations: CLSM, confocal laser scanning microscopy; DAPI, 4′,6-diamidino-2-phenylindole; DOX, doxorubicin; DOX·HCl, DOX hydrochloride; FA, folic acid; HA, hyaluronic acid; SD, standard deviation.

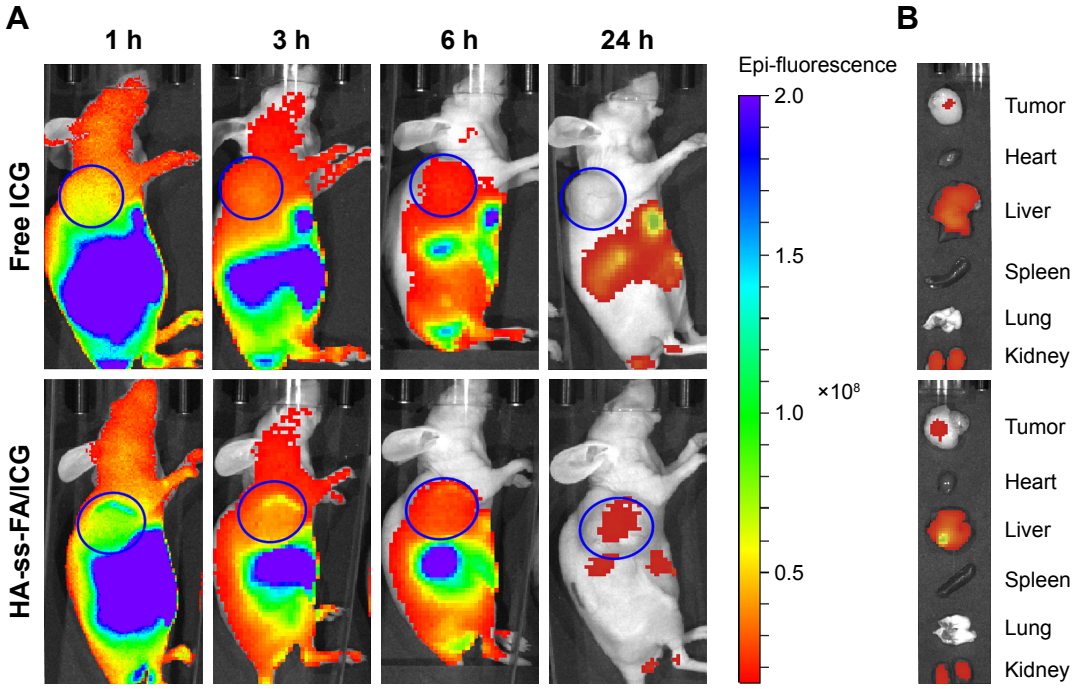

Figure 12 In vivo biodistribution studies of HA-ss-FA micelles.
Notes: (**A**) In vivo fluorescence images of HCCLM3 tumor-bearing nude mice at 1, 3, 6, and 24 h after tail vein injection of free ICG and HA-ss-FA/ICG micelles. (**B**) Ex vivo fluorescence images of tumor, heart, liver, spleen, lung, and kidney collected at 24 h after injection. The tumor regions are marked with blue circles.
Abbreviations: FA, folic acid; HA, hyaluronic acid; ICG, indocyanine green.

accumulation of ICG in the tumor region 1 h postinjection and the fluorescence of ICG-loaded micelles was 4- to 6.6-fold stronger than free ICG within 6 h. In addition, the ICG fluorescence in the tumor region still existed in the mice injected with ICG-loaded micelles 24 h postinjection, whereas there was no ICG fluorescence in the mice injected with free ICG. The result demonstrated that the micelles can improve HCCLM3 tumor-targeting ability of ICG in vivo.

The biodistribution of the micelles in organs was observed ex vivo. As shown in Figure 12B, the micelles were distributed mainly in tumor, kidney, and liver 24 h postinjection. Considerable accumulation of the micelles was found in liver. It is reported that HA hepatic clearance is mediated by the HARE receptor in liver sinusoidal endothelial cells, so HA and its derivatives located mostly in the liver.[63] There was obvious accumulation in kidney, too. Since urinary excretion is a route to eliminate the smaller Mw HA (~25 kDa),[64] the distribution of the micelles in the kidney seemed reasonable. The result was in accordance with previous reports.[57,65,66] The most accumulation of free ICG was in the liver, kidney, and tumor 24 h postinjection, due to the liver-specific distribution of ICG and the uptake of particulates by the reticuloendothelial system.[67,68]

Conclusion

In this study, we designed a reduction-sensitive CD44-positive tumor-targeted drug delivery system for DOX delivery. HA-ss-FA conjugate was synthesized and characterized. The mean diameter of blank and HA-ss-FA/DOX micelles was ~100–120 nm, the PDI was <0.3, and the zeta potential was negative. The DOX-loaded micelles were of high EE (88.09%) and DL (22.70%). HA-ss-FA had excellent biocompatibility and no obvious cytotoxicity. HA-ss-FA/DOX micelles showed an increased release of DOX in reduction environment. Moreover, the micelles could enhance the cellular uptake of DOX in CD44 receptor-positive HCCLM3 cells and A549 cells and improved the tumor-targetability of DOX in HCCLM3 tumor-bearing nude mice. In summary, this reduction-sensitive delivery system is a potential strategy for CD44 receptor-targeted cancer therapy.

Acknowledgments

This study was supported by the programs of the National Natural Science Foundation of China (81403175), Xinglin Young Talent Program from Shanghai University of Traditional Chinese Medicine, Project from Shanghai Municipal Commission of Health and Family Planning (20134Y053 and M20170396), Youth Talent Sail Plan from Shanghai

Committee of Science and Technology (14YF1411300), and Research Fund for the Doctoral Program of Shanghai (B201703).

Disclosure

The authors report no conflicts of interest in this work.

References

1. Chan WCW, Khademhosseini A, Parak W, Weiss PS. Cancer: nanoscience and nanotechnology approaches. *ACS Nano*. 2017;11(5):4375–4376.
2. Hou J, Wang J, Sun E, et al. Preparation and evaluation of icariside II-loaded binary mixed micelles using Solutol® HS15 and Pluronic F127 as carriers. *Drug Deliv*. 2016;23(9):3248–3256.
3. Ojha T, Pathak V, Shi Y, et al. Pharmacological and physical vessel modulation strategies to improve EPR-mediated drug targeting to tumors. *Adv Drug Deliv Rev*. 2017;119:44–60.
4. Pedrosa SS, Pereira P, Correia A, Gama FM. Targetability of hyaluronic acid nanogel to cancer cells: in vitro and in vivo studies. *Eur J Pharm Sci*. 2017;104:102–113.
5. Guruprasath P, Kim J, Gunassekaran GR, et al. Interleukin-4 receptor-targeted delivery of Bcl-xL siRNA sensitizes tumors to chemotherapy and inhibits tumor growth. *Biomaterials*. 2017;142:101–111.
6. Jain D. Cardiotoxicity of doxorubicin and other anthracycline derivatives. *J Nucl Cardiol*. 2000;7(1):53–62.
7. Shoukry HS, Ammar HI, Rashed LA, et al. Prophylactic supplementation of resveratrol is more effective than its therapeutic use against doxorubicin induced cardiotoxicity. *PLoS One*. 2017;12(7):e0181535.
8. Li K, Zhang Y, Chen M, et al. Enhanced antitumor efficacy of doxorubicin-encapsulated halloysite nanotubes. *Int J Nanomedicine*. 2018;13:19–30.
9. Thorn CF, Oshiro C, Marsh S, et al. Doxorubicin pathways: pharmacodynamics and adverse effects. *Pharmacogenet Genomics*. 2010;21(7):440–446.
10. Ammar HI, Saba S, Ammar RI, Elsayed LA, Ghaly WB, Dhingra S. Erythropoietin protects against doxorubicin-induced heart failure. *Am J Physiol Heart Circ Physiol*. 2011;301(6):2413–2421.
11. Shah K, Crowder D, Overmeyer J, Maltese W, Yun Y. Hyaluronan drug delivery systems are promising for cancer therapy because of their selective attachment, enhanced uptake, and superior efficacy. *Biomed Eng Lett*. 2015;5(2):109–123.
12. Kheiri Manjili H, Ghasemi P, Malvandi H, Mousavi MS, Attari E, Danafar H. Pharmacokinetics and in vivo delivery of curcumin by copolymeric mPEG-PCL micelles. *Eur J Pharm Biopharm*. 2017;116:17–30.
13. Guan J, Zhou ZQ, Chen MH, et al. Folate-conjugated and pH-responsive polymeric micelles for target-cell-specific anticancer drug delivery. *Acta Biomater*. 2017;60:244–255.
14. Liu Y, Fu S, Lin L, et al. Redox-sensitive Pluronic F127-tocopherol micelles: synthesis, characterization, and cytotoxicity evaluation. *Int J Nanomedicine*. 2017;12:2635–2644.
15. Wu JZ, Bremner DH, Li HY, Sun XZ, Zhu LM. Synthesis and evaluation of temperature- and glucose-sensitive nanoparticles based on phenylboronic acid and N-vinylcaprolactam for insulin delivery. *Mater Sci Eng C Mater Biol Appl*. 2016;69:1026–1035.
16. Arpicco S, Milla P, Stella B, Dosio F. Hyaluronic acid conjugates as vectors for the active targeting of drugs, genes and nanocomposites in cancer treatment. *Molecules*. 2014;19(3):3193–3230.
17. Tran TH, Choi JY, Ramasamy T, et al. Hyaluronic acid-coated solid lipid nanoparticles for targeted delivery of vorinostat to CD44 overexpressing cancer cells. *Carbohydr Polym*. 2014;114:407–415.
18. Yan H, Song J, Jia X, Zhang Z. Hyaluronic acid-modified didecyldimethylammonium bromide/d-a-tocopheryl polyethylene glycol succinate mixed micelles for delivery of baohuoside I against non-small cell lung cancer: in vitro and in vivo evaluation. *Drug Deliv*. 2017;24(1):30–39.
19. Wickens JM, Alsaab HO, Kesharwani P, et al. Recent advances in hyaluronic acid-decorated nanocarriers for targeted cancer therapy. *Drug Discov Today*. 2016;22(4):665–680.
20. Han X, Dong X, Li J, et al. Free paclitaxel-loaded E-selectin binding peptide modified micelle self-assembled from hyaluronic acid-paclitaxel conjugate inhibit breast cancer metastasis in a murine model. *Int J Pharm*. 2017;528(1–2):33–46.
21. Cho HJ, Yoon HY, Koo H, et al. Self-assembled nanoparticles based on hyaluronic acid-ceramide (HA-CE) and Pluronic® for tumor-targeted delivery of docetaxel. *Biomaterials*. 2011;32(29):7181–7190.
22. Lehner R, Liu K, Wang X, Hunziker P. Efficient receptor mediated siRNA delivery in vitro by folic acid targeted pentablock copolymer-based micelleplexes. *Biomacromolecules*. 2017;18(8):2654–2662.
23. Ramya AN, Joseph MM, Maniganda S, Karunakaran V, Sreelekha TT, Maiti KK. Emergence of gold-mesoporous silica hybrid nanotheranostics: Dox-encoded, folate targeted chemotherapy with modulation of SERS fingerprinting for apoptosis toward tumor eradication. *Small*. Epub 2017 Jul 3;13(31).
24. Kaur A, Jain K, Mehra NK, Jain NK. Development and characterization of surface engineered PPI dendrimers for targeted drug delivery. *Artif Cells Nanomed Biotechnol*. 2016;45(3):414–425.
25. Liu Y, Sun J, Lian H, Cao W, Wang Y, He Z. Folate and CD44 receptors dual-targeting hydrophobized hyaluronic acid paclitaxel-loaded polymeric micelles for overcoming multidrug resistance and improving tumor distribution. *J Pharm Sci*. 2014;103(5):1538–1547.
26. Zhao H-X, Yang C-X, Yan X-P. Fabrication and bioconjugation of BIII and CrIII co-doped ZnGa2O4 persistent luminescent nanoparticles for dual-targeted cancer bioimaging. *Nanoscale*. 2016;8(45):18987–18994.
27. Liu Y, Sun J, Cao W, et al. Dual targeting folate-conjugated hyaluronic acid polymeric micelles for paclitaxel delivery. *Int J Pharm*. 2011;421(1):160–169.
28. Zhao X, Jia X, Liu L, et al. Double-cross-linked hyaluronic acid nanoparticles with pH/reduction dual-responsive triggered release and pH-modulated fluorescence for folate-receptor-mediated targeting visualized chemotherapy. *Biomacromolecules*. 2016;17(4):1496–1505.
29. Xiong XY, Pan X, Tao L, et al. Enhanced effect of folated pluronic F87-PLA/TPGS mixed micelles on targeted delivery of paclitaxel. *Int J Biol Macromol*. 2017;103:1011–1018.
30. Deng B, Xia M, Qian J, et al. Calcium phosphate-reinforced reduction-sensitive hyaluronic acid micelles for delivering paclitaxel in cancer therapy. *Mol Pharm*. 2017;14(6):1938–1949.
31. Dong X, Liu C. Preparation and characterization of self-assembled nanoparticles of hyaluronic acid-deoxycholic acid conjugates. *J Nanomater*. 2010;2010:9.
32. Zhu Z, Hao X, Yan M, et al. Cancer stem/progenitor cells are highly enriched in CD133+CD44+ population in hepatocellular carcinoma. *Int J Cancer*. 2010;126(9):2067–2078.
33. Ganesh S, Iyer AK, Gattacceca F, Morrissey DV, Amiji MM. In vivo biodistribution of siRNA and cisplatin administered using CD44-targeted hyaluronic acid nanoparticles. *J Control Release*. 2013;172(3):699–706.
34. Oliveira AV, Marcelo A, Costa AM, Silva GA. Evaluation of cystamine-modified hyaluronic acid/chitosan polyplex as retinal gene vector. *Mater Sci Eng C Mater Biol Appl*. 2016;58:264–272.
35. Santhanam S, Liang J, Baid R, Ravi N. Investigating thiol-modification on hyaluronan via carbodiimide chemistry using response surface methodology. *J Biomed Mater Res A*. 2015;103(7):2300–2308.
36. Mulcahy EM, Fargierlagrange M, Mulvihill DM, O'Mahony JA. Characterisation of heat-induced protein aggregation in whey protein isolate and the influence of aggregation on the availability of amino groups as measured by the ortho-phthaldialdehyde (OPA) and trinitrobenzenesulfonic acid (TNBS) methods. *Food Chem*. 2017;229:66–74.
37. Adler-Nissen J. Determination of the degree of hydrolysis of food protein hydrolysates by trinitrobenzenesulfonic acid. *J Agric Food Chem*. 1979;27(6):1256.

38. Chen YH, Wang Q. Establishment of CTAB turbidimetric method to determine hyaluronic acid content in fermentation broth. *Carbohydr Polym*. 2009;78(1):178–181.
39. Santoveña A, Monzón C, Delgado A, Evora C, Llabrés M, Fariña JB. Development of a standard method for in vitro evaluation of triamcinolone and BMP-2 diffusion mechanism from thermosensitive and biocompatible composite hyaluronic acid-pluronic hydrogels. *J Drug Deliv Sci Technol*. 2017;42:284–291.
40. Zhong Y, Zhang J, Cheng R, et al. Reversibly crosslinked hyaluronic acid nanoparticles for active targeting and intelligent delivery of doxorubicin to drug resistant CD44+ human breast tumor xenografts. *J Control Release*. 2015;205:144–154.
41. Kang Y, Lu L, Lan J, et al. Redox-responsive polymeric micelles formed by conjugating gambogic acid with bioreducible poly(amido amine)s for the co-delivery of docetaxel and MMP-9 shRNA. *Acta Biomater*. 2018;68:137–153.
42. Sun C, Li X, Du X, Wang T. Redox-responsive micelles for triggered drug delivery and effective laryngopharyngeal cancer therapy. *Int J Biol Macromol*. 2018;112:65–73.
43. Qin B, Liu L, Wu X, et al. mPEGylated solanesol micelles as redox-responsive nanocarriers with synergistic anticancer effect. *Acta Biomater*. 2017;64:211–222.
44. Li Y, Tian B, Yang J, et al. Stepwise metastatic human hepatocellular carcinoma cell model system with multiple metastatic potentials established through consecutive in vivo selection and studies on metastatic characteristics. *J Cancer Res Clin Oncol*. 2004;130(8):460–468.
45. Council NR. *Guide for the Care and Use of Laboratory Animals*. Washington, DC: The National Academies Press; 1996.
46. Welti D, Rees DA, Welsh EJ. Solution conformation of glycosaminoglycans: assignment of the 300-MHz 1H-magnetic resonance spectra of chondroitin 4-sulphate, chondroitin 6-sulphate and hyaluronate, and investigation of an alkali-induced conformation change. *Eur J Biochem*. 1979;94(2):505–514.
47. Gilli R, Kacuráková M, Mathlouthi M, Navarini L, Paoletti S. FTIR studies of sodium hyaluronate and its oligomers in the amorphous solid phase and in aqueous solution. *Carbohydr Res*. 1994;263(2):315–326.
48. Saadat E, Shakor N, Gholami M, Dorkoosh FA. Hyaluronic acid based micelle for articular delivery of triamcinolone, preparation, in vitro and in vivo evaluation. *Int J Pharm*. 2015;489(1–2):218–225.
49. Zheng S, Jin Z, Han J, et al. Preparation of HIFU-triggered tumor-targeted hyaluronic acid micelles for controlled drug release and enhanced cellular uptake. *Colloids Surf B Biointerfaces*. 2016;143:27–36.
50. Blanco E, Shen H, Ferrari M. Principles of nanoparticle design for overcoming biological barriers to drug delivery. *Nat Biotechnol*. 2015;33(9):941.
51. Xiao K, Li Y, Luo J, et al. The effect of surface charge on in vivo biodistribution of PEG-oligocholic acid based micellar nanoparticles. *Biomaterials*. 2011;32(13):3435–3446.
52. Alexis F, Pridgen E, Molnar LK, Farokhzad OC. Factors affecting the clearance and biodistribution of polymeric nanoparticles. *Mol Pharm*. 2008;5(4):505–515.
53. Tian C, Asghar S, Xu Y, et al. The effect of the molecular weight of hyaluronic acid on the physicochemical characterization of hyaluronic acid-curcumin conjugates and in vitro evaluation in glioma cells. *Colloids Surf B Biointerfaces*. 2018;165:45–55.
54. Dosio F, Arpicco S, Stella B, Fattal E. Hyaluronic acid for anticancer drug and nucleic acid delivery. *Adv Drug Deliv Rev*. 2016;97:204–236.
55. Liu GY, Li M, Zhu CS, Jin Q, Zhang ZC, Ji J. Charge-conversional and pH-sensitive PEGylated polymeric micelles as efficient nanocarriers for drug delivery. *Macromol Biosci*. 2014;14(9):1280–1290.
56. Liu H, Wu S, Yu J, et al. Reduction-sensitive micelles self-assembled from amphiphilic chondroitin sulfate A-deoxycholic acid conjugate for triggered release of doxorubicin. *Mater Sci Eng C Mater Biol Appl*. 2017;75:55–63.
57. Li J, Huo M, Wang J, et al. Redox-sensitive micelles self-assembled from amphiphilic hyaluronic acid-deoxycholic acid conjugates for targeted intracellular delivery of paclitaxel. *Biomaterials*. 2012;33(7):2310–2320.
58. Zhong Y, Goltsche K, Cheng L, et al. Hyaluronic acid-shelled acid-activatable paclitaxel prodrug micelles effectively target and treat CD44-overexpressing human breast tumor xenografts in vivo. *Biomaterials*. 2016;84:250–261.
59. Zhu Y, Zhang J, Meng F, et al. cRGD-functionalized reduction-sensitive shell-sheddable biodegradable micelles mediate enhanced doxorubicin delivery to human glioma xenografts in vivo. *J Control Release*. 2016;233:29–38.
60. Ke XY, Lin NV, Gao SJ, Tong YW, Hedrick JL, Yang YY. Co-delivery of thioridazine and doxorubicin using polymeric micelles for targeting both cancer cells and cancer stem cells. *Biomaterials*. 2014;35(3):1096–1108.
61. Wang L, Tian B, Jing Z, et al. Coordinated pH/redox dual-sensitive and hepatoma-targeted multifunctional polymeric micelle system for stimuli-triggered doxorubicin release: synthesis, characterization and in vitro evaluation. *Int J Pharm*. 2016;501(1–2):221–235.
62. Saneja A, Nayak D, Srinivas M, et al. Development and mechanistic insight into enhanced cytotoxic potential of hyaluronic acid conjugated nanoparticles in CD44 overexpressing cancer cells. *Eur J Pharm Sci*. 2017;97:79–91.
63. Tripodo G, Trapani A, Torre ML, Giammona G, Trapani G, Mandracchia D. Hyaluronic acid and its derivatives in drug delivery and imaging: recent advances and challenges. *Eur J Pharm Biopharm*. 2015;97(pt B):400–416.
64. Kuehl C, Zhang T, Kaminskas LM, et al. Hyaluronic acid molecular weight determines lung clearance and biodistribution after instillation. *Mol Pharm*. 2016;13(6):1904–1914.
65. Thomas RG, Moon M, Lee S, Jeong YY. Paclitaxel loaded hyaluronic acid nanoparticles for targeted cancer therapy: in vitro and in vivo analysis. *Int J Biol Macromol*. 2015;72:510–518.
66. Choi KY, Min KH, Na JH, et al. Self-assembled hyaluronic acid nanoparticles as a potential drug carrier for cancer therapy: synthesis, characterization, and in vivo biodistribution. *J Mater Chem*. 2009;19(24):4102–4107.
67. Zheng M, Yue C, Ma Y, et al. Single-step assembly of DOX/ICG loaded lipid – polymer nanoparticles for highly effective chemo-photothermal combination therapy. *ACS Nano*. 2013;7(3):2056–2067.
68. Zhang J, Jin W, Wang X, Wang J, Zhang X, Zhang Q. A novel octreotide modified lipid vesicle improved the anticancer efficacy of doxorubicin in somatostatin receptor 2 positive tumor models. *Mol Pharm*. 2010;7(4):1159–1168.

Supplementary materials

Table S1 ^{1}H NMR data of HA-ss-FA conjugate

Number	δ_H (ppm)		
	HA	CYS	FA
1	4.27–4.32	–	–
2	3.34	–	–
3	3.58	–	–
4	3.74	–	–
5	3.70	–	–
6	4.55	–	–
7	3.82	–	–
8	3.71	–	–
9	3.51	–	–
10	3.47	–	–
11 proR	3.68	–	–
11 proS	3.90	–	–
a	2.01	–	–
b	–	3.00	–
c	–	2.85	–
d	–	–	8.75
e	–	–	7.92
f	–	–	7.65
g	–	–	6.81

Note: "–" indicates no data.
Abbreviations: CYS, cystamine; FA, folic acid; HA, hyaluronic acid; NMR, nuclear magnetic resonance.

Table S2 FTIR data of HA-ss-FA conjugate

cm^{-1}	Proposed assignments	
	HA	FA
3,270 (s)	ν(O–H) H bonded	ν(O–H) H bonded
2,887 (m)	ν(C–H)	–
1,603 (s)	νas(C–O)[COOH]	νas(C–O)[COOH] bonded
1,451 (m)	νs(C–O)[COOH]	–
1,402–1,300 (m)	δ(C–H)[CH_2]	δ(C–H)[CH2]
1,031 (s)	ν(C–OH)	–
1,507 (sh)	–	C–C stretch (in-ring) aromatics
832 (sh)	–	Ar–H

Note: "–" indicates no data.
Abbreviations: Ar–H, aromatic hydrogen; FA, folic acid; FTIR, Fourier transform infrared; HA, hyaluronic acid; s, strong; m, medium, sh, sharp.